Acta Biomaterialia 10 (2014) 2056–2064

Contents lists available at ScienceDirect

Acta Biomaterialia

journal homepage: www.elsevier.com/locate/actabiomat

Organic interlamellar layers, mesolayers and mineral nanobridges: Contribution to strength in abalone (*Haliotis rufescence*) nacre

Maria I. Lopez [a,*], Pedro E. Meza Martinez [b], Marc A. Meyers [a,b,c]

[a] *Materials Science and Engineering Program, University of California, San Diego, La Jolla, USA*
[b] *Department of Mechanical and Aerospace Engineering, University of California, San Diego, La Jolla, USA*
[c] *Department of Nanoengineering, University of California, San Diego, La Jolla, USA*

ARTICLE INFO

Article history:
Received 25 July 2013
Received in revised form 25 November 2013
Accepted 9 December 2013
Available online 15 December 2013

Keywords:
Nacre
Mesolayers
Organic constituent
Red abalone
Mineral bridges

ABSTRACT

The contributions of mesolayers, organic interlamellar layers and nanoasperities/mineral bridges to the strength of nacre from red abalone (*Haliotis rufescens*) shell nacre are investigated. Samples were demineralized and deproteinized to separate the organic and mineral components, respectively. Tensile tests were performed on both the isolated organic constituent and the isolated mineral. The strength of the isolated organic component suggests that growth bands play an important role in the mechanical behavior as they are thick regions of protein that are a significant fraction (~0.4) of the total organic content. The thickness variation of the nacre tablets was measured and found to be a small fraction of the mean tablet thickness (0.568 μm); the standard deviation is 26 nm, indicating that the wedge mechanism of toughening does not operate in the nacre investigated. Results obtained from the isolated mineral validate the importance of the organic constituent as the mechanical properties decline greatly when the organic component is removed. The results presented herein add to the understanding of the mechanical response of the organic interlayers and growth bands and their effect on the toughness of the abalone nacre.

1. Introduction

Nacre is a natural composite that exhibits exceptional mechanical properties due to its structural organization that extends to various levels of hierarchy. Most of the toughness has been previously attributed to the brick-and-mortar structure consisting of $CaCO_3$ tablets (~0.5 μm thick) interconnected by mineral nanobridges [1] and separated by organic interlayers (~20–50 nm thick) (Fig. 1a). However, there are other important levels of hierarchy such as that of growth bands (also known as mesolayers) that appear in abalone (*Haliotis*) due to feeding and temperature fluctuations [2]. Aragonitic $CaCO_3$ constitutes the inorganic component of the nacreous composite present in many mollusks [3–7]. Fig. 1b shows partially demineralized nacre that exposes the organic interlayer covering the tablets. This "nanolayer" has holes that grow upon stretching at a rate that is significantly larger than the biaxial stretching [8].

Mesolayers are ~20 μm thick layers (~20 μm thick) of organic material which appear approximately every 300 μm separating regions of regular platelet stacking [3,5,8,9]. It has been demonstrated by Sullivan and Prorok that shells grown commercially at constant temperatures do not possess these growth bands [10]. Fig. 1a shows a mesolayer that was formed between the brick-and-mortar nacre structure during seasonal fluctuations. Fig. 1c shows a partially demineralized nacre specimen exposing the mesolayers within the nacreous structure consisting of a thick layer of organic material in which minerals are embedded [5].

The organic interlayer in nacre has been the subject of considerable structural and mechanical investigations [8,11–16]. This organic matrix consists of β-chitin fibrils having a diameter of ~20 nm surrounded by acidic macromolecules that attach themselves to the top and bottom surface of the tablets [17,18]. The organic interlayer appears to be periodically deposited (every ~0.5 μm) by the epithelial layer. This membrane (20–60 nm) is permeable allowing the flow of Ca^{2+} and CO_2^{-3} ions, so that lateral growth can continue until the gap between adjacent tablets closes. The holes also allow a continuous growth between the mineral layers by the formation of mineral bridges [19]. These mineral nanoscale bridges and asperities play an important role in the formation of the microstructure and the overall mechanical properties and have been studied widely [4,8,9,20–25]. Previous transmission electron microscopy work and selected-area diffraction patterns [26,27] show that the crystal orientation does not change significantly between a tablet to the adjacent tablet. This high degree of crystallographic alignment normal to the plane of the tablets

* Corresponding author. Tel.: +1 9158202824.
E-mail addresses: mil032@ucsd.edu, mlopezfierro4@gmail.com (M.I. Lopez).

1742-7061/$ - see front matter © 2013 Acta Materialia Inc. Published by Elsevier Ltd. All rights reserved.
http://dx.doi.org/10.1016/j.actbio.2013.12.016

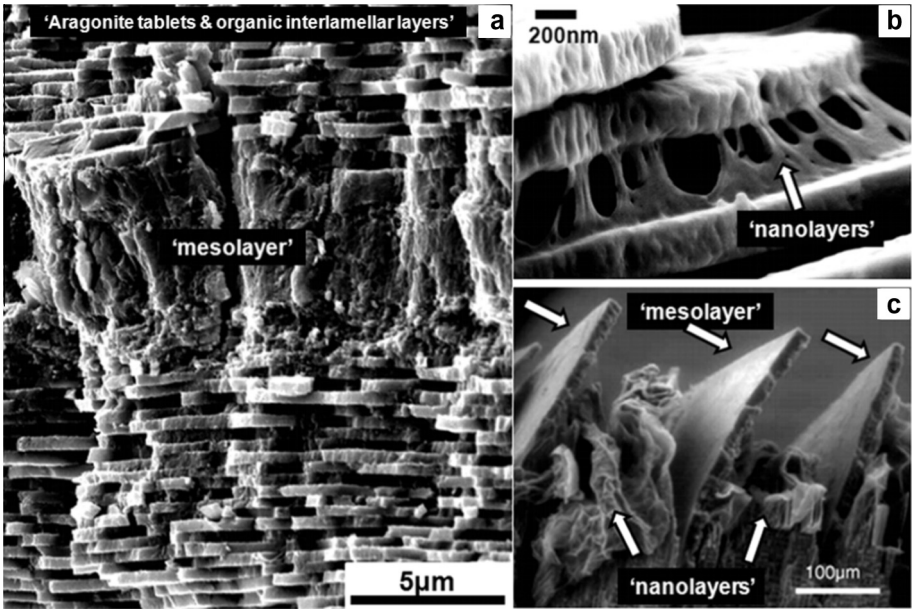

Fig. 1. (a) Fracture surface of red abalone nacre showing the brick-and-mortar architecture separated by a mesolayer, or growth band. (b) Partially demineralized nacre exposing the tent-like organic membrane. (c) Mesolayers and nanolayers (collapsed) within a partially demineralized nacreous structure consisting of a thick layer of organic material with an embedment of minerals. (Adapted from Lin and Meyers [5].)

is attributed to the belief that the growth of consecutive layers of tablets is formed and mediated through a series of porous organic membranes [8,11,19,23,28]. In addition, they provide the tensile strength in the direction perpendicular to the layered structure. It was proposed that these bridges, having a diameter of ranging from 20 to 60 nm, do not have their tensile strength determined by the critical crack size, but by the theoretical strength. Their number is such that the tensile strength of the tablets (parallel to the tablet/shell surface plane) is optimized for a tablet thickness of 0.5 μm, as proposed by Lin and Meyers [5]. Additionally, they contribute to the shear strength of the tablets and are important in the pull-out process.

A limited number of studies have been performed on the mechanical properties of the organic interlamellar layers. Semi-quantitive evaluation of the strength was conducted based on the sag exhibited by the dry organic layer held between terraced cones [8]. These results suggested low values of flow strength, and viscoelastic behavior of the organic interlayer. On the other hand, nanoindentation measurements performed on the dry organic layer [11] demonstrated that such layers exhibited considerable resistance. For these experiments a Berkovich tip was lowered and touched the organic matrix before encountering the mineral tablet. The load–displacement curves demonstrated a drastic change from when the tip penetrates the top of the tablet in comparison to when it encounters the organic matrix. The latter situation results in a curve that exhibits a plateau at a load of ~100 μN, corresponding to the resistance of one dry organic layer. These measurements were used to estimate the resistance of the organic layer to deformation and/or failure. There was a significant increase in strength from the values obtained by measuring the sag in the membrane [8], attributed to the high sensitivity of the structure to the degree of hydration.

Monotonic tensile and time-dependent relaxation experiments performed by Bezares et al. [15] revealed that the interlamellar organic layers followed a constitutive response conforming to a viscoelastic standard linear solid. These results, however, failed to include the effects of the thick organic mesolayers, which may in fact have an affect on the overall toughness of the nacre. More recently, Dastjerdi et al. [29] performed tensile tests on the isolated organic layers of three different shell types: pearl oyster, top shell and red abalone. The first two did not contain mesolayers, whereas the shell of red abalone did. The results suggest that growth lines (mesolayers) play an important role in the mechanical behavior. The organic material in the abalone shell provided higher stiffness compared to the other shells.

One of the objectives of the present research is to establish the role of the organic interlayers and, especially, of the mesolayers, on the mechanical properties. An additional goal is to evaluate the contribution of the mineral bridges to the overall tensile strength when the load is applied perpendicular to the tablet layers.

2. Materials and methods

2.1. Shell sectioning

Two fresh abalone shells from animals that were previously held and raised in an open water tank at the facility at the Scripps Institution of Oceanography at La Jolla, CA were sectioned for tensile testing of demineralized nacre. Abalones were hand selected directly from the open water tank and immediately frozen overnight at ~−20 °C (with the animal still attached to the shell). During the following week, the animal was detached from the shell and the shell was directly sectioned (all sectioning and grinding was performed with the shell hydrated); the shell specimens were then embedded in a acrylic resin and immersed in EDTA solution. Following demineralization, the organic constituent was washed and maintained in deionized (DI) water to avoid the structure from becoming dry, brittle or losing flexibility. During tensile testing, the specimens were continuously misted with DI water to ensure they remained hydrated. Specimens were cut and polished in rectangular sections of 12.5 mm × 6 mm; the thickness was varied (Fig. 2a, c) in order to control the number of mesolayers per specimen. The calcitic layer was removed via wet grinding (confirmed by optical microscopy), leaving only the nacreous layer. The sectioning was performed by aligning the longitudinal axis of the specimens with the logarithmic growth direction lines (Fig. 2a). Additional grinding and polishing were carried out to achieve with close precision a

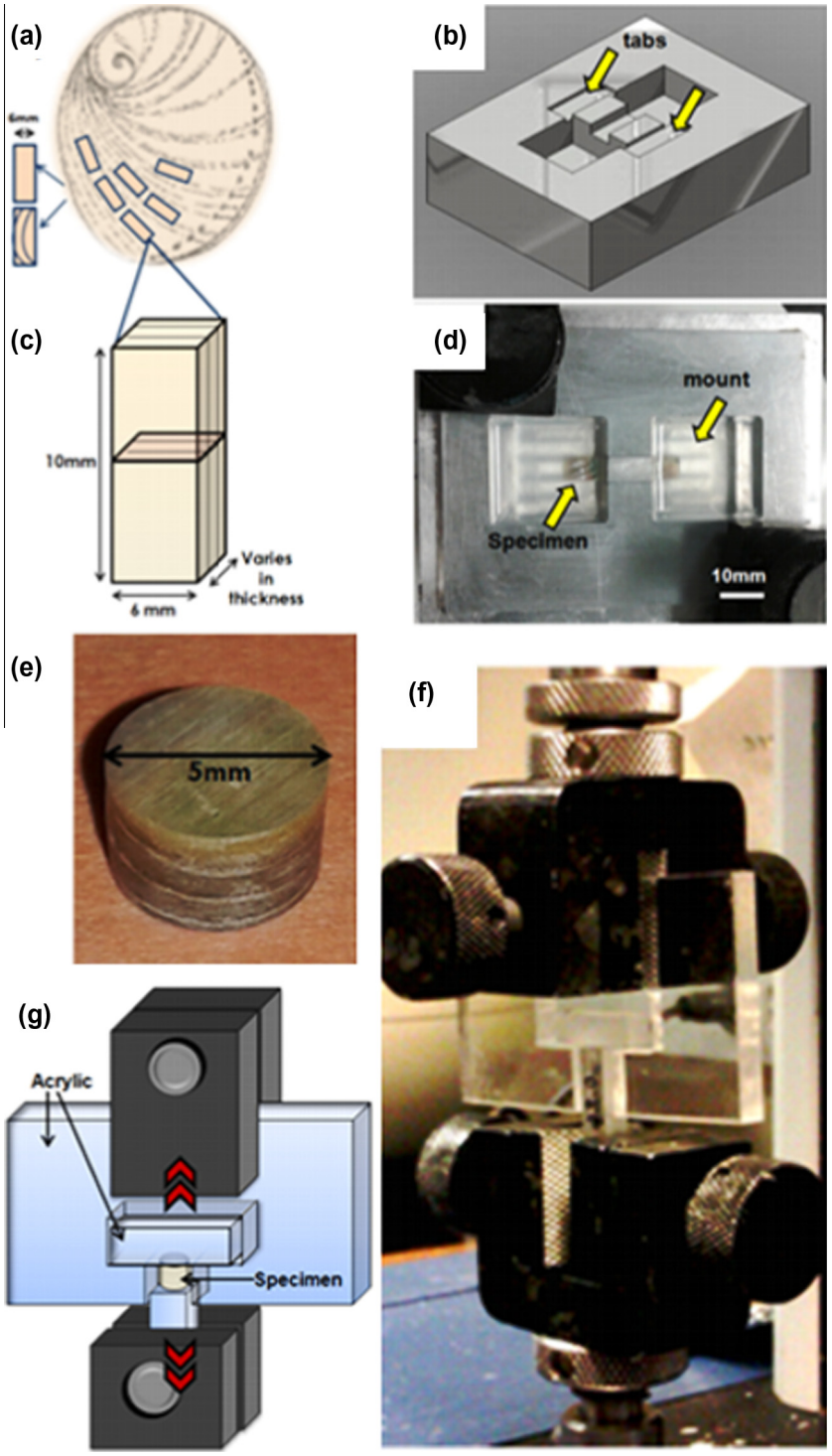

Fig. 2. (a, c) Schematic of shell sectioning orientation and specimen dimensions. (b) Schematic of mounting mold designed to provide easier handling of demineralized specimens. (d) Sample embedded in epoxy inside the mold. (e) Drilled puck of untreated nacre. (f, g) Actual tensile design setup and schematic representation to pull apart the untreated and deproteinized pucks while minimizing bending.

parallel alignment between the specimen surface and the shell growth surfaces. This was done in order to ensure there was an engagement of the layers and to minimize damage during the demineralization process. Furthermore, the sections were ground in thickness to control and approximate the number of organic interlamellar layers and to vary the number of mesolayers in each specimen. By varying the thickness it is possible to obtain both specimens that contain mesolayers and some specimens that do not have them.

Shell sectioning for tensile testing of deproteinized nacre was performed by drilling cylindrical pucks of nacre, 5 mm in diameter, from fresh abalone shells using a diamond coring drill in a procedure described previously by Meyers et al. [8]. Care was taken to make lateral surfaces perpendicular to the concavity of the surface

of the shell (Fig. 1a) to ensure that the inner nacre layers were as parallel to the ends of the cylindrical specimen as possible. Specimens were then ground and polished to remove the external calcitic layer and to create flat ends. The thickness of these specimens varied from 0.3 to 3 mm.

2.2. Embedding and mount setup

Preliminary demineralization nacre studies demonstrated that the response is very sensitive to the tensile test arrangement. Previous studies [15] used an elegant setup, in which the edges of untreated nacre were first embedded, exposing a specific section of the nacre that was then demineralized. However, this study also suggested that significant damage was caused by the embedding and handling of the demineralized nacre. As the nacre is demineralized, the integrity of the specimens is decreased and they become pliable and prone to tearing. It is the calcium carbonate that provides the majority of the stiffness in nacre; when removed, any mishandling of the exposed organic constituent can damage the specimen.

To avoid further problems in the handling and immobilizing of the specimens prior to testing, a specialized mounting mold was designed (Fig. 2b, d). The untreated nacre specimens (of various thicknesses) are positioned in the center of the mold, and only the edges are embedded in the acrylic, exposing the central region (10 mm long $\times$ 6 mm wide) of the specimen and allowing it to undergo demineralization when in contact with the solution. To ensure easy handling of the demineralized nacre, the edges of the mount remain connected by two thin tabs of acrylic. Then, once the mount edges are engaged and positioned in the machine grips for testing and the entire test setup is ready, the two thin tabs are cut, allowing for the load to be applied only to the demineralized nacre.

For the testing of the mineral bridges of nacre, a special setup was also created to reduce the damage that can occur to the cylindrical specimens (pucks) prior to testing. Once nacre loses all of its organic constituents it becomes brittle and fragile. To reduce any preloading prior to testing, the pucks were mounted in an acrylic setup that allowed the sample to be gripped and handled of the sample (Fig. 2f, g). In this setup, the tensile load was applied perpendicular to the tablets. With the removal of the organic constituent, the load is applied only to the mineral.

2.3. Demineralization and peproteinization

Embedded untreated nacre specimens were demineralized using the method described by Bezares et al. [14], utilizing 0.6 M EDTA at a pH of 8.0. Once demineralized, specimens were placed in DI water for 24 h prior to testing to ensure that they were hydrated. Demineralized specimens where examined visually to identify mesolayers since they appear much darker visually than the organic interlamellar layers when demineralized. Area fraction and particle size (either pore size or asperity top-surface area) measurements were performed with ImageJ software. Scanning electron microscopy (SEM) images of the same resolution were taken of flat areas of "bird's-eye views" of the fracture surfaces of the deproteinized nacre and of demineralized nacre. The grayscale image was then converted to binary and then split into channels, and pixels in the different areas were counted. A total of 1707 asperities were measured from the deproteinized nacre and a total of 1681 nanopores were measured to compute the area fraction. Furthermore, 140 asperities and 95 pores were magnified and precisely measured to obtain an average radius.

Removal of all organic material from the original nacre was performed by submerging the specimen in 0.5 N NaOH at 20 °C for 10 days under constant, gentle shaking. After deproteinization, sample pucks were observed via SEM to confirm that the mineral structure was still intact.

2.4. Mechanical testing

Tensile testing was performed on a tabletop desktop Instron 3342 system at strain rates of 10^{-2} and 10^{-4} s^{-1}. The load was applied parallel to the organic layers in the demineralized specimens and perpendicular to the tablet layers in the deproteinized pucks.

2.5. Scanning electron and optical microscopy

Subsequent to mechanical testing, the ruptured demineralized specimens were sectioned and dehydrated completely in a progressive manner in ethanol and CO_2 critical point dried so that the structure was preserved. Samples were gold–platinum coated and observed in a FEI SFEG ultrahigh-resolution scanning electron microscope. Sections of the edge of the nacre that was embedded in the acrylic and that was not exposed to the demineralizing solution were cut, polished, and observed via SEM and optical microscopy. The interface between the demineralized and untreated nacre served as a guideline of the structure prior to the demineralization and allowed the number of mesolayers in each specimen to be accurately determined. The fracture surface of tested isolated mineral (puck) specimens was also observed by SEM.

3. Results

We present the results of three experimental procedures: (i) tensile tests on organic layer (Secs. 3.1 and 3.2); (ii) tensile tests perpendicular to tablet orientation (Secs. 3.3 and 3.4); (iii) aragonite tablet thickness measurements (Sec. 3.5).

3.1. Demineralized nacre: structural observations

Fig. 3 shows an optical micrograph (post-demineralization) of a cross-sectional cut exposing the interface between the demineralized and the untreated nacre. It should be noted that the section of the nacre specimen remained intact, retaining its original geometry. This confirms that the embedding procedure was successful in exposing only the desired section of the nacre to the demineralizing solution while ensuring a good grip on the untreated edge. As the removal of the mineral proceeds, the organic interlamellar layers are exposed and a loss of integrity occurs. However, the thicker mesolayers do not exhibit such a loss of integrity. Fig. 3 shows three mesolayers (identified by arrows) that retain some stiffness, unlike the interlamellar organic nanolayers that aggregate between them due to their much lower thickness (~20 nm vs. ~20 μm). These observations enable the number of mesolayers

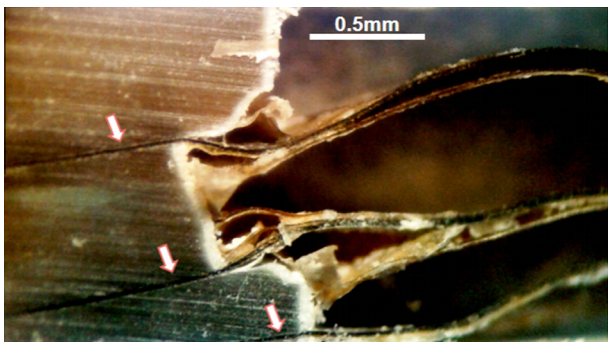

Fig. 3. Interface between demineralized and untreated nacre, showing three mesolayers (depicted by arrows) that retain stiffness, unlike organic interlayers that crumble and aggregate in between.

present in each specimen to be determined, which is necessary for the calculation of cross-sectional area.

Fig. 4 illustrates a view of this sequence of layers. Fig. 4a shows the individual tablet imprints obtained after demineralization. Further inspection (Fig. 4b) shows five successive layers (numbered 1–5) that collapse on top of each other after demineralization. The porous structure is the result of a network of fibers. The pores have an average radius of ~20 nm with a standard deviation of 8 nm.

3.2. Demineralized nacre: mechanical properties

The axial stress was calculated by approximating the number of organic layers (both nano and meso) that would be contained in each specimen. Given that the specimen thickness varied from 0.18 to 3 mm, the amount of organic constituent can vary considerably among specimens. The number of nanolayers present in each specimen was estimated by considering the original (untreated) thickness of each specimen and assuming that an interlayer of 20 nm thick exists for every aragonite tablet.

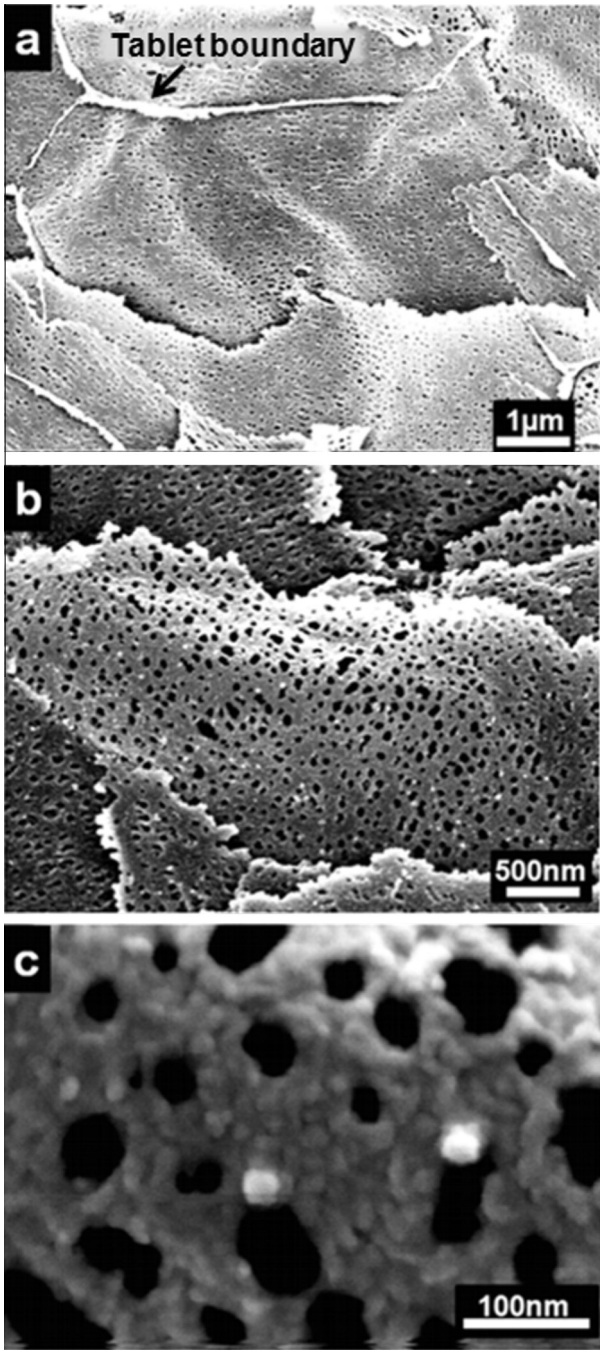

Fig. 4. Demineralized nacre exposing organic interlayers: (a) overall view of layers showing tablet boundaries; (b) sequence of five layers (1–5); (c) higher resolution of layers exposing "nanopores" with an average diameter 23 nm.

The results of tensile tests are shown in Fig. 5. Specimens were tested at strain rates of 10^{-2} and $10^{-4}\ s^{-1}$, at 20 °C, while water was continuously misted over them, ensuring that demineralized nacre remained hydrated throughout the duration of the test. The number of thick organic mesolayers was estimated by optical microscopy, and varied from zero to five; they are indicated in each specimen beside its plot. The elastic modulus was estimated and its values are in the ranges $12.5\ \text{MPa} \leqslant E \leqslant 115\ \text{MPa}$ and $1\ \text{MPa} \leqslant E \leqslant 7.2\ \text{MPa}$ for the 10^{-2} and $10^{-4}\ s^{-1}$ strain rates, respectively. These results (Fig. 5) show that demineralized nacre exhibits a rate-dependent behavior. It is possible to estimate this viscoelastic behavior from the equation:

$$E = C\dot{\epsilon}^{d} \tag{1}$$

which is commonly applied to biological materials, especially bone, and is known as the Ramberg–Osgood equation. Assuming values of E of 50 and 3.5 MPa at the strain rates of 10^{-2} and $10^{-4}\ s^{-1}$, respectively, the value of the exponent d is 0.57.

3.3. Isolated mineral: structural observations

Fig. 6 shows a cross-sectional view of nacre after deproteinization. The mineral tablets remain completely intact, retaining their ~500 nm thickness and shape (Fig. 6a). In Fig. 6b two edges of neighboring tablets can be observed; one can note nanoasperities (shown by arrows) in close proximity (if not connecting) the upper and lower tablets.

Subsequent to tensile testing, the fracture surface of the puck was observed via SEM. Fig. 6c, d shows one of these surfaces (taken from a "bird's-eye view"). Different tablet layers (depicted by arrows) are peeled off as the load is applied. Closer inspection of this surface (Fig. 6d) reveals nanoasperities that cover the entire tablet face. The asperities have an average diameter of ~29 nm and cover the surface with a uniform distribution. The average diameter of the asperities approximates well to the nanopore diameter in the organic interlamellar layer (Fig. 4c).

3.4. Isolated mineral: mechanical properties

Fig. 7 shows the Weibull analysis of nacre under quasi-static tension with the load perpendicular to the layers. While the Weibull distribution [30] is usually used for flexural strength and is representative of extreme-value statistics, here it is applied to a variety of quasi-tensile data with intention of creating a clear picture from a scattered range of data points. The Weibull analysis [30] was applied by means of the equation:

$$F(V) = 1 - \exp\left[-\left(\frac{\sigma}{\sigma_0}\right)^{m}\right], \tag{2}$$

which can be transformed into:

$$\ln\ln\left[\frac{1}{1-F(V)}\right] = m(\ln\sigma - \ln\sigma_0), \tag{3}$$

where $F(V)$ is the failure probability, m is the Weibull modulus and σ_o is a characteristic strength. The parameters σ_o and m are experimentally obtained by plotting the two sides of Eq. (3) and finding the value of $\ln\sigma$ at which $\ln\ln\,[1/(1-F)]$ equals zero, and taking the slope of the best-fit line, respectively. The Weibull curve yields an S-shaped distribution from which the failure probability at a

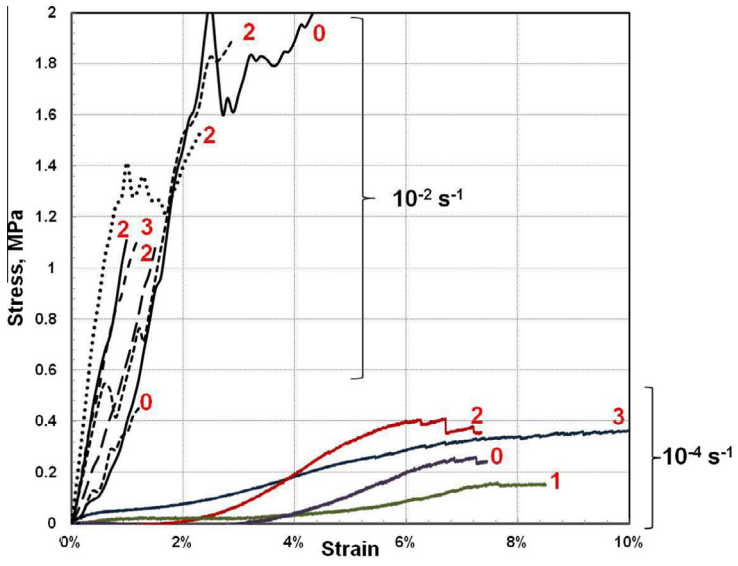

Figure 5. Quasi-static tensile tests of demineralized nacre with load applied parallel to organic layers. Number adjacent to each plot represents the number of mesolayers present in each specimen. Dashed lines represent specimens tested at a strain rate of 10^{-2} s^{-1} and lines represent specimens tested at a strain rate of 10^{-4} s^{-1}.

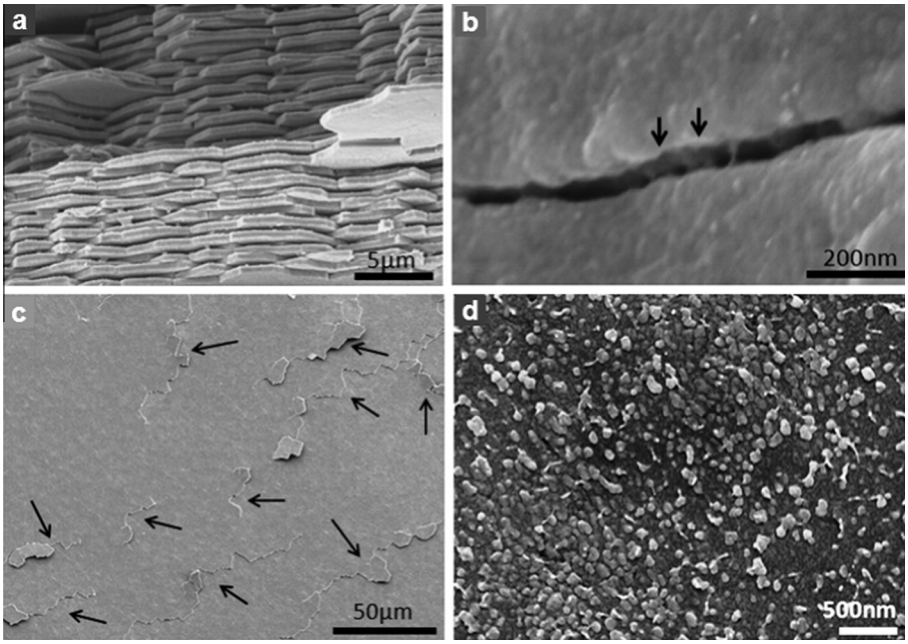

Fig. 6. (a) Cross-sectional view of the post-deproteinized nacre retaining structure of mineral tablets (~500 nm in thickness). (b) Neighboring tablets exposing nanoasperities on upper and lower tablets. (c) "Bird's-eye view" of fracture surface showing different tablet layers peeled off as load is applied. (d) Nanoasperities covering the surface in a uniform distribution.

specific stress can be computed. In general, we can describe the 50% failure probability as the characteristic strength of the material, although σ_o (the value for $F(V) = 1/e$) is also used.

The current results, presented in Fig. 7, predict a 50% failure probability occurring at ~0.325 MPa for tension perpendicular to the layered structure. This value is extremely low, especially when we consider that the tensile strength perpendicular to the layer plane for untreated nacre is of the order of 3–4 MPa (plotted in the figure as well as values from Ref. [8]) These results are consistent with the ones by Lin et al. [8] for which at 50% failure probability occurs at 4.1 MPa.

3.5. Thickness variation of tablets

The aragonite tablet size and shape has been a topic of debate. The tablet thickness has been estimated to be 0.4–0.5 μm [31]. For the purpose of this study, simple quantification of the tablet thickness was performed. Fig. 8a shows a back-scatter electron microscopy (BSEM) image of a polished surface of nacre depicting horizontal organic layers (dark lines) where the thickness measurements where performed. Fig. 8b–f shows a series of measurements of the thickness over several layers. The tablet thickness averaged 0.56 μm with a standard deviation of 26 nm. The shape

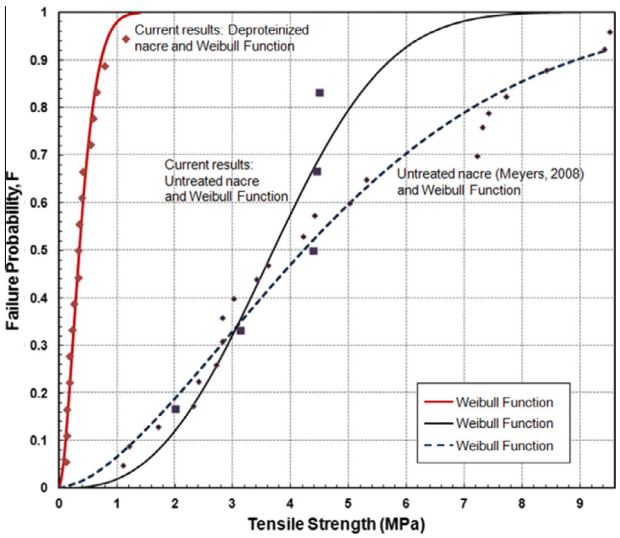

Fig. 7. Weibull distribution of tensile strength perpendicular to layered structure of current untreated nacre, deproteinized nacre, and compared to previous results obtained by Meyers et al. [8]. Curve on left represents the failure probability of the deprotenized nacre. The areal basis for computing the strength corresponds to 18% of the total area; this is the estimated fraction of occupied by mineral bridges.

of the tablets has been previously described as "wedged" [32–35] rather than flat. This was proposed to play a role in the shear strength of the nacre by inhibiting inter-tablet sliding and tablet pull-out. However, the current results suggest a different explanation. The thickness is plotted vs. displacement on five adjacent tablet layers. For each separate layer, the plot has a unique pattern, showing that some tablet areas might be slightly thicker than others. However, if tablets had a "wedge" shape, this would be visible in the plot and would create a periodicity in every layer (as depicted in the hypothetical case in Fig. 8g).

4. Discussion

4.1. Demineralized nacre

Weibull statistics are employed to characterize the results and compare them to those previously obtained by Bezares et al. [15]. Fig. 9 presents statistical summaries of Bezares et al.'s mechanical tests on demineralized nacre under quasi-static tension, with failure probabilities of 50% being reached at ~3.1 MPa. The strain rate used by Bezares et al. [13] was 10^{-4} s^{-1}. In comparison, the failure probability of 50% obtained here (Fig. 9: current, nano and mesolayers) is ~1.1 MPa. This difference in value is due to the incorporation of mesolayers into the area calculation, something not considered by Bezares et al. [15] when computing the axial stress. As comparison, the axial stress of the current data were recomputed assuming mesolayers were non-existent (Fig. 9: current, nanolayers). Using this method, the tensile strength values increase to 2.5 MPa and approximate those values attained by Bezares et al. [15] (Fig. 9: Bezares et al., 2010).

As mentioned earlier, the formation of mesolayers can be induced by fluctuations in temperature and feeding [2]. When temperature drops, mineralization is arrested, allowing for the formation of a mesolayer. Thus, it is believed that in many cases farmed abalone do not experience these temperature fluctuations

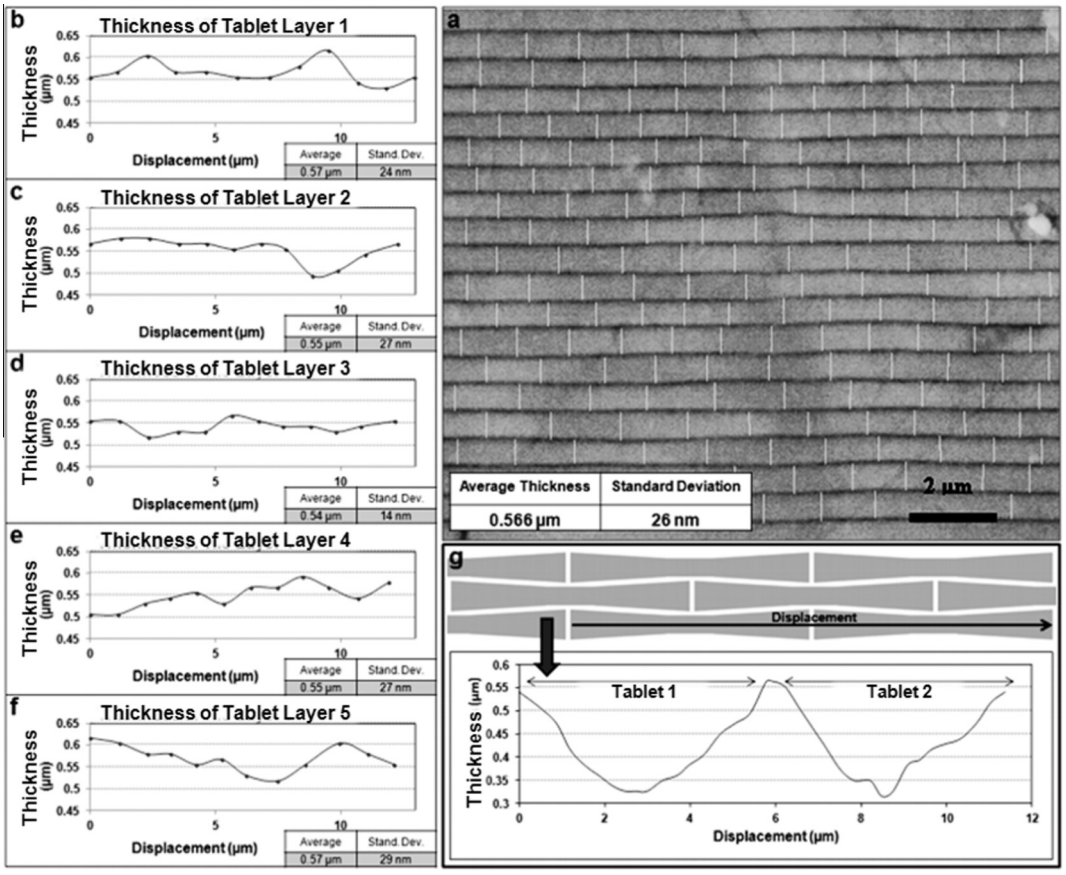

Fig. 8. (a) BSEM of polished surface showing horizontal organic layers (dark lines). Note the vertical lines separating tablets laterally are not (or only faintly) visible. (b–f) Thickness variation of five adjacent tablet layers. (g) Schematic and thickness variation if tablets were wedge-shaped.

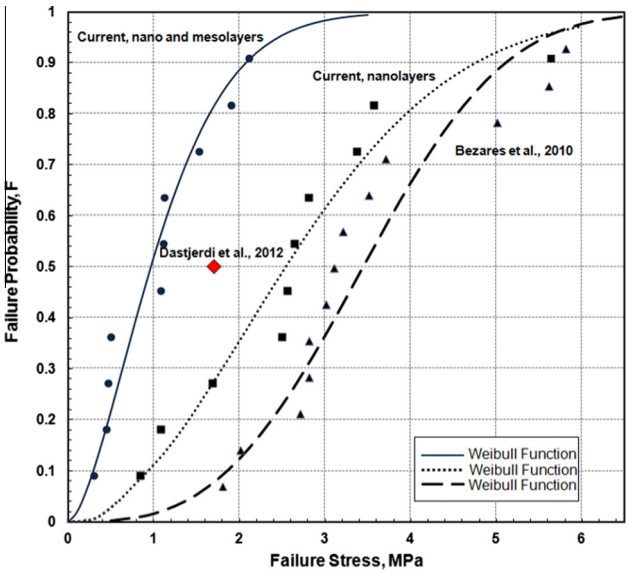

Fig. 9. Weibull distribution of tensile strength of organic component showing: current results (including nano and mesolayers), results presented by Bezares et al. [5] (Bezares et al. (2010)) and what the values here would look like assuming that no mesolayers were present (Current, nanolayers). Additionally a diamond point was added to reflect findings by Dastjerdi et al. [26], who reported the average strength of the material to be ~1.75 MPa.

and thus not form mesolayers. Shaw et al. [10] report observations on farmed abalone in which no mesolayers are present. In the current study, the abalone were obtained from the Scripps Institute of Oceanography open water facilities where they were exposed to natural water temperature fluctuations similar to those that wild abalone experience.

Dastjerdi et al. [29] tested three different shell types: red abalone, pearl oyster and top shell. Of these, only red abalone contains mesolayers. Their results show that lower strength values and higher failure strain values are attained for pearl oyster and top shell than red abalone. They claim this noticeable difference in modulus is a result of the mesolayers that are found in red abalone. Our results are in good agreement with those presented by Dastjerdi et al. [29] for abalone nacre (fail at a similar strength value), with a mean strength of 1.75 ± 0.5 MPa and a failure strain of 2 ± 1% (Fig. 9: Dastjerdi et al.). The failure process seen here was similar to Dastjerdi et al.'s results, exhibiting first the delamination of mesolayers, when they are present in the specimen, followed by a failure normal to the growth line. It is interesting to note that the stress–strain response (Fig. 5) is similar irrespective of whether or not the specimens contain mesolayers. This suggests that the organic nanolayers and mesolayers have the same mechanical response.

4.2. Isolated mineral

A comparison between the structural observations of isolated organic material and the isolated mineral allows us to make some interesting observations. The pores found within the organic interlamellar layer enable (i) the flow of ions to continue the mineralization process and (ii) the formation of mineral bridges between adjacent tablet layers. Given that this is the fracture surface of the tested specimens, some of the nanoasperities are indeed fractured mineral bridges. The asperities on the surface of the mineral tablets and the holes within the organic matrix sheet were quantified. The average radius of the the pores is ~20 nm (standard deviation of 8 nm) compared to that of the asperities, which is ~33 nm (standard deviation of 16 nm). This difference in diameter might be because as the nacre is demineralized the nanopores in the organic interlamellar layer are no longer stressed and thus are able to shrink. Hence, the pores are somewhat stretched by the nanoasperities when the entire nacre structure is intact. Previous studies show that mineral bridges appear as circular columns with diameters of ~38–54 nm [36] and ~25–55 nm [37], while the pores exhibit diameters ranging from 5 to 50 nm. The average diameter of the nanoasperities measured here is larger than these previous reported values, but the average value for the pore diameter is in good agreement with results by Song and Bai [1].

There is still debate as to the fraction of asperities that actually connect to form mineral bridges. Gries et al. [37] and Checa et al. [38] suggest than in some cases these asperities do not connect but only protrude from neighboring tablets. Current results show that the nanoasperities cover ~33% of the surface of the mineral tablets, compared to the area provided by the pores, which is estimated to be ~18%. The discrepancy between total area occupied by the nanoasperities to that of the pores suggests that only a fraction of the nanoasperities are mineral bridges. This might also justify the difference in diameter size between pores and nanoasperities. Furthermore, the areal fraction covered by the pores in the organic interlamellar layer (~18% of tablet surface area) is similar to values estimated by Song and Bai [1] (~15% of the surface area of the tablets). This in turn provides a better estimated value of the area that is covered by "true" mineral bridges. Calculations by Song and Bai [1] provide a value of ~1,600 mineral bridges per tablet (tablet diagonal ~1.8–6.2 μm); here we estimate ~3,000 nanoasperities per tablet (tablet diagonal ~8 μm). Additionally, Song and Bai [1] propose that the average density distribution of mineral bridges varies, decreasing from the center to the periphery of the tablets. In contrast, the current observations show a uniform distribution of nanoasperities throughout the entire surface area of the tablets.

Mineral bridges are believed to regulate the tensile strength (perpendicular to the shell surface), thus increasing the fracture toughness by controlling the crack extension pattern in nacre [8,36]. The current results, presented in Fig. 7, predict a 50% failure probability occurring at ~0.325 MPa for tension perpendicular to the layered structure. Note that the stresses given in this curve correspond to the average of the mineral bridges assumed that 18% of area is occupied by the latter. This is an extremely low value compared to the hypothesized theoretical value. The mineral bridges (~40 nm in diameter and ~20 nm in height) approach the critical scale for monocrystal aragonite which is ~30 nm. Thus, the strength should be reaching the theoretical value, which for monocrystal aragonite is ~3.3 GPa. However, in the current experiments, the material reaches far below that value, thus implying that the material is not defect free. There are three possible reasons for this: (i) the existence of an organic phase embedded in the mineral and

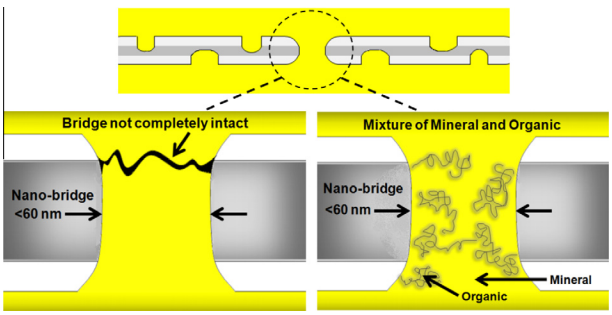

Fig. 10. Schematic of mineral bridges. A representation of a mineral bridge containing organic component which can be deteriorated during the deproteinization process and the representation of a mineral bridge that may not be intact and thus not contributing to the strength of the nacre when tested in tension perpendicularly to the tablet layers.

the organic material surrounding the mineral bridges [22,39] deteriorates the integrity of the bridges during the deproteinization process, leading to the creation of cracks or defects in the mineral bridges (Fig. 10a); (ii) some of the mineral bridges/connections are damaged or broken prior to testing, lowering their strength (Fig. 10b); (iii) the usually observed protrusions are not in fact mineral bridges.

5. Conclusions

The principal conclusions that can be drawn from the current research are as follows:

1. We have established the tensile strength of the organic interlayer (both nano and meso) and estimate it to be ~2 MPa at 10^{-2} s^{-1}.
2. Whereas the tensile strengths of abalone nacre parallel and perpendicular to the tablet layer are ~100–150 MPa and ~3–5 MPa, respectively, the tensile strength of the organic layer is of the order of 2 MPa. Thus, the inherent resistance of the organic nanolayer and mesolayer contribute little to the overall strength. Their primary purpose is to subdivide the aragonite matrix and thereby control the crack propagation path.
3. The organic interlamellar layer has high strain-rate sensitivity, characteristic of hydrated organic composites: ~0.3–0.5.
4. A significant fraction (~0.4) of the nanoasperities correspond to protrusions on the surface, and do not form mineral bridges.
5. The distribution and density of the nanopores within the organic interlamellar layer provide a better estimate of the number of mineral bridges.

Acknowledgements

This research is supported by the National Science Foundation Grant DMR 1006931 and a Ford Foundation Pre-Doctoral Fellowship. We thank Ryan Anderson for his assistance at the Calit^2 facility. Discussions with Professors Joanna McKittrick and Po-Yu Chen are gratefully acknowledged. We dedicate this paper to Jiddu Bezares, who passed away tragically and unexpectedly shortly before completing his Ph.D. He gave his time generously to us and inspired us with his knowledge and experience.

Appendix A. Figures with essential colour discrimination

Certain figures in this article, particularly Figs. 2, 3, 5, 7, 9, 10 are difficult to interpret in black and white. The full colour images can be found in the on-line version, at doi: http://dx.doi.org/10.1016/j.actbio.2013.12.016

References

[1] Song F, Bai YL. Mineral bridges of nacre and its effects. Acta Mech Sinica 2001;17:251–7.
[2] Lopez MI, Chen PY, McKittrick J, Meyers MA. Growth of nacre in abalone: seasonal and feeding effects. Mat Sci Eng C Mater 2011;31:238–45.
[3] Menig R, Meyers MH, Meyers MA, Vecchio KS. Quasi-static and dynamic mechanical response of *Haliotis rufescens* (abalone) shells. Acta Mater 2000;48:2383–98.
[4] Barthelat F, Li CM, Comi C, Espinosa HD. Mechanical properties of nacre constituents and their impact on mechanical performance. J Mater Res 2006;21:1977–86.
[5] Lin A, Meyers MA. Growth and structure in abalone shell. Mat Sci Eng A Struct 2005;390:27–41.
[6] Li XD, Chang WC, Chao YJ, Wang RZ, Chang M. Nanoscale structural and mechanical characterization of a natural nanocomposite material: the shell of red abalone. Nano Lett 2004;4:613–7.
[7] Fleischli FD, Dietiker M, Borgia C, Spolenak R. The influence of internal length scales on mechanical properties in natural nanocomposites: a comparative study on inner layers of seashells. Acta Biomater 2008;4:1694–706.
[8] Meyers MA, Lin AYM, Chen PY, Muyco J. Mechanical strength of abalone nacre: role of the soft organic layer. J Mech Behav Biomed 2008;1:76–85.
[9] Su XW, Belcher AM, Zaremba CM, Morse DE, Stucky GD, Heuer AH. Structural and microstructural characterization of the growth lines and prismatic microarchitecture in red abalone shell and the microstructures of abalone "flat pearls". Chem Mater 2002;14:3106–17.
[10] Shaw GA, Prorok B, Starman LA. MEMS and nanotechnology, vol. 6. New York, London: Springer; 2012.
[11] Meyers MA, Lim CT, Li A, Nizam BRH, Tan EPS, Seki Y, et al. The role of organic intertile layer in abalone nacre. Mat Sci Eng C Mater 2009;29:2398–410.
[12] Checa AG, Rodriguez-Navarro AB. Self-organisation of nacre in the shells of Pterioida (Bivalvia: Mollusca). Biomaterials 2005;26:1071–9.
[13] Cartwright JHE, Checa AG. The dynamics of nacre self-assembly. J R Soc Interface 2007;4:491–504.
[14] Bezares J, Asaro RJ, Hawley M. Macromolecular structure of the organic framework of nacre in *Haliotis rufescens*: implications for growth and mechanical behavior. J Struct Biol 2008;163:61–75.
[15] Bezares J, Asaro RJ, Hawley M. Macromolecular structure of the organic framework of nacre in *Haliotis rufescens*: implications for mechanical response. J Struct Biol 2010;170:484–500.
[16] Yao N, Epstein AK, Liu WW, Sauer F, Yang N. Organic–inorganic interfaces and spiral growth in nacre. J R Soc Interface 2009;6:367–76.
[17] Sarikaya M, Gunnison KE, Yasrebi M, Aksay JA. Mechanical property-microstructural relationships in abalone shell. Materials synthesis utilizing biological processes. Mater Res Soc 1990;174:109–66.
[18] Levi-Kalisman Y, Falini G, Addadi L, Weiner S. Structure of the nacreous organic matrix of a bivalve mollusk shell examined in the hydrated state using cryo-TEM. J Struct Biol 2001;135:8–17.
[19] Schaffer TE, IonescuZanetti C, Proksch R, Fritz M, Walters DA, Almqvist N, et al. Does abalone nacre form by heteroepitaxial nucleation or by growth through mineral bridges? Chem Mater 1997;9:1731–40.
[20] Song F, Zhang XH, Bai YL. Microstructure and characteristics in the organic matrix layers of nacre. J Mater Res 2002;17:1567–70.
[21] Song F, Bai YL. Effects of nanostructures on the fracture strength of the interfaces in nacre. J Mater Res 2003;18:1741–4.
[22] Rousseau M, Lopez E, Stempfle P, Brendle M, Franke L, Guette A, et al. Multiscale structure of sheet nacre. Biomaterials 2005;26:6254–62.
[23] Lin AY, Chen PY, Meyers MA. The growth of nacre in the abalone shell. Acta Biomater 2008;4:131–8.
[24] Saruwatari K, Matsui T, Mukai H, Nagasawa H, Kogure T. Nucleation and growth of aragonite crystals at the growth front of nacres in pearl oyster, *Pinctada fucata*. Biomaterials 2009;30:3028–34.
[25] Espinosa HD, Rim JE, Barthelat F, Buehler MJ. Merger of structure and material in nacre and bone – perspectives on de novo biomimetic materials. Prog Mater Sci 2009;54:1059–100.
[26] Feng QL, Cui FZ, Pu G, Wang RZ, Li HD. Crystal orientation, toughening mechanisms and a mimic of nacre. Mater Sci Eng 2000;11:19.
[27] DiMasi E, Sarikaya M. Synchrotron X-ray microbeam diffraction from abalone shell. J Mater Res 2004;19:1471–6.
[28] Cartwright JHE, Checa AG. The dynamics of nacre self-assembly. J R Soc Interface 2007;4:491–504.
[29] Dastjerdi AK, Rabiei R, Barthelat F. The weak interfaces within tough natural composites: experiments on three types of nacre. J Mech Behav Biomed 2013;19:50–60.
[30] Weibull W. A statistical distribution function of wide applicability. J Appl Mech T Asme 1951;18:293–7.
[31] Barthelat F. Biomimetics for next generation materials. Phil Trans R Soc A 2007;365:2907–19.
[32] Barthelat F, Tang H, Zavattieri PD, Li CM, Espinosa HD. On the mechanics of mother-of-pearl: a key feature in the material hierarchical structure. J Mech Phys Solids 2007;55:306–37.
[33] Barthelat F, Zhu DJ. A novel biomimetic material duplicating the structure and mechanics of natural nacre. J Mater Res 2011;26:1203–15.
[34] Barthelat F, Espinosa HD. An experimental investigation of deformation and fracture of nacre-mother of pearl. Exp Mech 2007;47:311–24.
[35] Espinosa HD, Juster AL, Latourte FJ, Loh OY, Gregoire D, Zavattieri PD. Tablet-level origin of toughening in abalone shells and translation to synthetic composite materials. Nat Commun 2011;2:190–211.
[36] Song F, Soh AK, Bai YL. Structural and mechanical properties of the organic matrix layers of nacre. Biomaterials 2003;24:3623–31.
[37] Gries K, Kroger R, Kubel C, Schowalter M, Fritz M, Rosenauer A. Correlation of the orientation of stacked aragonite platelets in nacre and their connection via mineral bridges. Ultramicroscopy 2009;109:230–6.
[38] Checa AG, Cartwright JH, Willinger MG. Mineral bridges in nacre. J Struct Biol 2011;176:330–9.
[39] Bezares J, Peng Z, Asaro RJ, Zhu Q. Macromolecular structure and viscoelastic response of the organic framework of nacre in *Haliotis rufescens*: a perspective and overview. J Theor Appl Mech 2011;38:75–106.